Special Contributions, Geophysical Institute, Kyoto University, No. 9, 1969, 137-166

CRUSTAL AND UPPER MANTLE STRUCTURE IN JAPAN FROM AMPLITUDE AND PHASE SPECTRA OF LONG-PERIOD P-WAVES

PART 2. KANTO PLAIN

By

Tuneto KURITA*

(Received October 11, 1967)

Abstract

Crustal and upper mantle structure in the Kanto plain has been investigated by the same method as described in Part 1 of this paper. Taking the amplitude ratio of the vertical component to the horizontal one of long-period P-waves registered at Tsukua and the phase difference between them, we obtain two observational curves related only to the structure beneath the Kanto plain. The curves for waves incident from almost due south are conspicuously different from those of the other directions, suggesting a difference in structure. Comparing seven sets of these curves corresponding to seven regions classified by the incident direction with the theoretical curves calculated by varying layer parameters of probable models derived so far from other studies we have obtained several models for each region. The most probable model has been selected on the assumption that the structure does not vary greatly with azimuth. This model has a crustal thickness of about 29 km and a thick 7.4 km/sec intermediate layer as much as 20 km or more. A comparison of travel-time residuals at Tsukuba with those at Matsushiro has revealed that at Tsukuba P-wave arrivals from the south to southwest direction are as much as 1 second earlier than those from the south to southeast direction. This has been reduced to a higher velocity in the upper mantle under the southwest part of the Kanto plain, compared with the velocity under the southeast part.

1. Introduction

The body wave method for determining the layered structure has been shown to be useful, as reviewed in Part 1 of this papar. Kurita [1969a] showed that, for determining the crustal and upper mantle structure, a comparison of the observational phase difference between the vertical and horizontal components with the corresponding theoretical one calculated by the Haskell-Thomson matrix method is really a powerful tool, as well as being a comparison between

* Department of Transportation Engineering, Faculty of Engineering, Kyoto University.

the observational and theoretical amplitude ratios. In this paper, using this method together with travel-time residuals, we shall determine the crustal and upper mantle structure in the Kanto plain in Japan from the analysis of seismograms recorded by long-period seismographs at Mt. Tsukuba.

2. Determination of observational curves

(1) *Data*

Data used in this study are contact copies of the seismograms recorded by the Columbia long-period seismographs at the Tsukuba Seismological Observatory (TSK) during the period from August, 1966 to December, 1968. The paper

Table 1. List of earthquakes and relevant information.

Shock Code	Origin Time Start of Analysis h m s	Location Lat. Long.	D[1] (km)	M[2]	Δ (deg)	Azim. (deg)	I_m (deg)	Phase Interval[3] (sec)	Length (sec)	Freq. Range (sec^{-1})	Q. R.[4]
NE 1	Dec. 17, 68 12 02 15.0 12 10 48	60.2N 152.8W Southern Alaska	86	5.9	48.2	38.2	33	P–PP 110	110	~0.150	B
NE 2	July 1, 67 23 10 07.2 23 18 25	54.4N 158.1W South of Alaska	N*	6.2	45.6	46.3	34±	P–PP 105	105		A
NE 3	May 27, 67 17 22 58.7 17 29 04	51.9N 176.1E Rat Islands	34R*	5.8	29.9	47.0	39±	P–PP 60 P–PcP 180	100		A
NE 4	June 19, 67 17 07 45.4 17 15 07	52.7N 166.9W Fox Islands	N*	5.7	40.3	48.7	35±	P–PP 95	95		A
SE 5	Mar. 11, 68 08 26 32.8 08 37 18	16.2S 173.9W Tonga Islands	112R*	6.0	67.8	131.8	26±	P–PP 150	100		B
SE 6	Aug. 12, 67 09 39 44.3 09 50 57	24.7S 177.5W South of Fiji Islands	134	5.8	72.6	140.0	24	P–pP 35	35	0.025~	C
SE 7	Sept. 26, 68 18 02 50.1 18 14 40	30.5S 178.2W Kermadec Islands Region	N	5.8	77.1	143.9	23±	P–PP 170	95	~0.160	B
SE 8	Oct. 28, 68 23 32 28.7 23 41 52	12.5S 166.4E Santa Cruz Islands	60G	5.9	54.4	147.8	31±	P–PP 120	110	0.025~ 0.125	B
SE 9	Oct. 7, 66 15 55 10.8 16 05 22	21.6S 170.5E Loyalty Islands Region	161R*	6.4	64.3	148.5	27±	P–PP 145	100		A
SE10	Nov. 12, 66 18 45 01.0 18 54 48	15.6S 167.3E New Hebrides Islands	40	5.2	57.6	148.6	30	P–PP 125	100		B

S E11	Sept. 12, 66 11 29 40.3 11 40 18	23.1S 170.6E Loyalty Islands Region	49	6.1	65.6	149.1	27	P-PP	145	65	0.045～	C
S S E 12	Sept. 28, 67 04 56 56.3 05 05 01	6.6S 153.4E New Britain Region	44R*	5.9	44.4	160.9	34±	P-PP	105	105	0.035～ 0.190	B
S S E 13	Mar. 7, 68 13 22 16.6 13 30 11	5.9S 151.1E New Britain Region	39	5.6	43.1	163.9	35	P-PP	100	100	～0.125	B
S W14	Sept. 8, 66 21 15 52.8 21 22 36	2.4N 128.4E Halmahera	96	6.9	35.3	200.4	34	P-PP	80	80		B
S W15	Oct. 14, 68 02 58 47.8 03 10 10	31.5S 117.0E Western Australia	0	6.0	70.8	200.8	26+	P-PP	155	100	0.030～	A
S W16	Aug. 4, 68 11 41 24.9 11 47 38	6.6N 126.8E Mindanao	107	5.7	31.9	205.7	38	P-sP	35	35		C
S W17	June 7, 68 11 57 29.5 12 05 18	1.8S 120.1E Celebes	20	5.9	42.1	210.6	35	P-PP	100	100		C
S W18	Mar. 24, 67 09 00 19.5 09 08 13	6.0S 112.4E Java Sea	600R	6.0	49.4	217.6	31	P-pP	110	110	0.025～ 0.150	A
W S W 19	May 21, 67 18 45 11.7 18 54 00	1.0S 101.5E Southern Sumatra	173R*	6.3	51.6	232.9	31±	P-sP	55	55		C
W S W 20	Aug. 21, 67 07 33 00.6 07 42 04	3.6N 95.8E Off West Coast of Northern Sumatra	N*	5.9	52.1	242.1	32±	P-PcP	80	80	～0.140	C
W 21	Sept. 28, 66 14 00 22.9 14 07 05	27.4N 100.1E Yunnan Province	N*	6.2	34.9	267.0	37±	P-PP	80	80	～0.120 0.145～	B
W 22	Aug. 30, 67 04 22 01.5 04 28 36	31.7N 100.3E Szechwan Province	3	6.1	33.2	273.9	38+	P-PP	65	65	0.030～	B
W N W 23	Aug. 31, 68 10 47 37.4 10 58 15	34.0N 59.0E Iran	13	6.0	64.5	294.5	27+	P-PP	140	100	～0.160 0.185～	B
W N W 24	Sept. 1, 68 07 27 30.2 07 38 10	34.0N 58.2E Iran	15	5.9	65.0	294.9	27+	P-PP	140	100	0.025～ 0.150	A
W N W 25	Aug. 19, 66 12 22 09.6 12 33 38	39.2N 41.7E Turkey	26R*	6.1	73.9	306.9	24±	P-PP	165	100	0.025～ 0.180 0.185～	B

Note; [1] The depth notation is according to the USCGS: N; Normal, R; Restraint, G; Geophysicist.

[2] Magnitude is according to the USCGS.

[3] Phase interval is mainly based on the Jeffreys-Bullen travel-time tables.

[4] Quality of Record.

speed was 15 mm/min and digitization was made at an interval shorter than 1.0 seconds. Table 1 is the list of the earthquakes analyzed and their relevant information. The code of the shock indicates the approximate direction of wave approach to Tsukuba, as shown in Fig. 1. Shocks with code NE (4 shocks) took place in the Alaska Peninsula to the Aleutian Islands. Shocks with code SE (7 shocks) and SSE (2 shocks) took place in the Southern Pacific region, and those with code SW (5 shocks) and WSW (2 shocks) in Indonesia, Australia and the Philippines. Shocks with code W (2 shocks) and WNW (3 shocks) took place in China, and Iran and Turkey respectively. Shocks SE9, SE11, W21 and WNW25 correspond to SE6, SE8, WNW11 and WNW15 in Part 1 respectively. The incident angle, i_m to the Moho around Tsukuba was obtained from $(i_d - \Delta)$ curve of Ritsema [1958]. "Phase Interval", which means the time interval between two successive incident phases, is based on the Jeffreys-Bullen travel-time tables and the tables of Herrin *et al.* [1968]. "Frequency Range" means the range within which the amplitude spectrum of a signal is several times greater than that of microtremors preceding the signal. The observational curves may be reliable within this frequency range. The rank A, B and C in the "Quality of Record" is a measure of reliability of the observational curves. The curves with rank A are reliable in the sense that sharp incidence of later phases is not recognized in time interval of analysis of about 100 seconds, which is long enough not to distort the resultant spectra. In the observational curves with rank B, the incidence of later phases is noticeable in the interval of analysis, but does not greatly damage the resultant observational curves. On the other hand, in rank C, there are some uncertainties in the peak positions of observational curves, since the time interval of analysis is generally limited due to sharp incidence of a later phase.

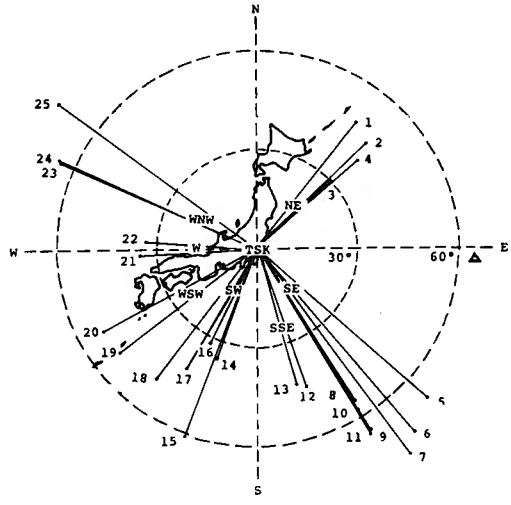

Fig. 1. Epicentral distance and azimuth of the earthquakes at Tsukuba. The scale of the figure of Japan is about four times larger than that of epicentral distance.

(2) *Analytical Procedure*

The analytical procedure adopted in this paper is almost the same as in

Part 1, with regard to utilized data windows, correction for the instrumental response and the method for determining the time interval of analysis. In this procedure, we superpose a data window on the signal and then Fourier analyze it, correcting the instrumental response. In the due order of analysis, however, we should superpose a data window on the waveform corrected by the instrumental response, and then Fourier analyze it. A comparison between these two cases is made in an article by Kurita [1969b], in which it is shown that for a "heavy" data window, $W_1(t)$, the difference in the resultant spectra is small and appears in rather higher frequencies for a time interval of analysis as long as 100 seconds or more, but it becomes appreciable for a time interval as short as 50 seconds. Consequently, in the case of a short time interval, this fact and the lowering of spectral resolution should be taken into consideration.

As listed in Table 1, an excellent observational curve has been obtained for the data window of $W_1(t)$ and the time interval of analysis of about 100 seconds. This may be due to the fact that in this case the major part of P phase with its reverberations in the layered strata mostly within 60 seconds is contained with a sufficient amplitude, and that the amplitude of later phases, if any, is supressed. If the time interval of analysis is extended to as long as 130 seconds, undulations generally become conspicuous in the observational curves. For a time interval within 70 seconds as indicated in Table 1, the observational curves with the data window $W_2(t)$ are considered most reliable. Taking these curves as a first approximation, the most reliable observational curves have been determined for each shock by superposing the data windows, $W_1(t)$ and $W_2(t)$ and by varying the time interval of analysis.

Observational curves thus obtained have been classified into seven groups according to the direction of wave approach as shown in Fig. 1, and plotted on lineprinter papers in Figs. 2, 3, 4, 5, 6, 7 and 8. In these figures, the observational curves with rank C in Table 1 are drawn by dash-pot lines. Dotted parts of the curves are beyond the "Frequency Range" in Table 1. When the observational curves are out of the ordinate range prescribed on the figures, they are condensed into that range.

Table 2. Instrumental parameters of Columbia long-period seismgraph operated at Tsukuba (140°06'36"E, 36°12'39"N, height 286m).

Component	Maximum Magnification	T_1 (sec)	T_2 (sec)	h_1	h_2	σ
UD	700	14.4	90	2.0	1.2	
NS	1400	15.0	102			
EW	1400	15.2	93			

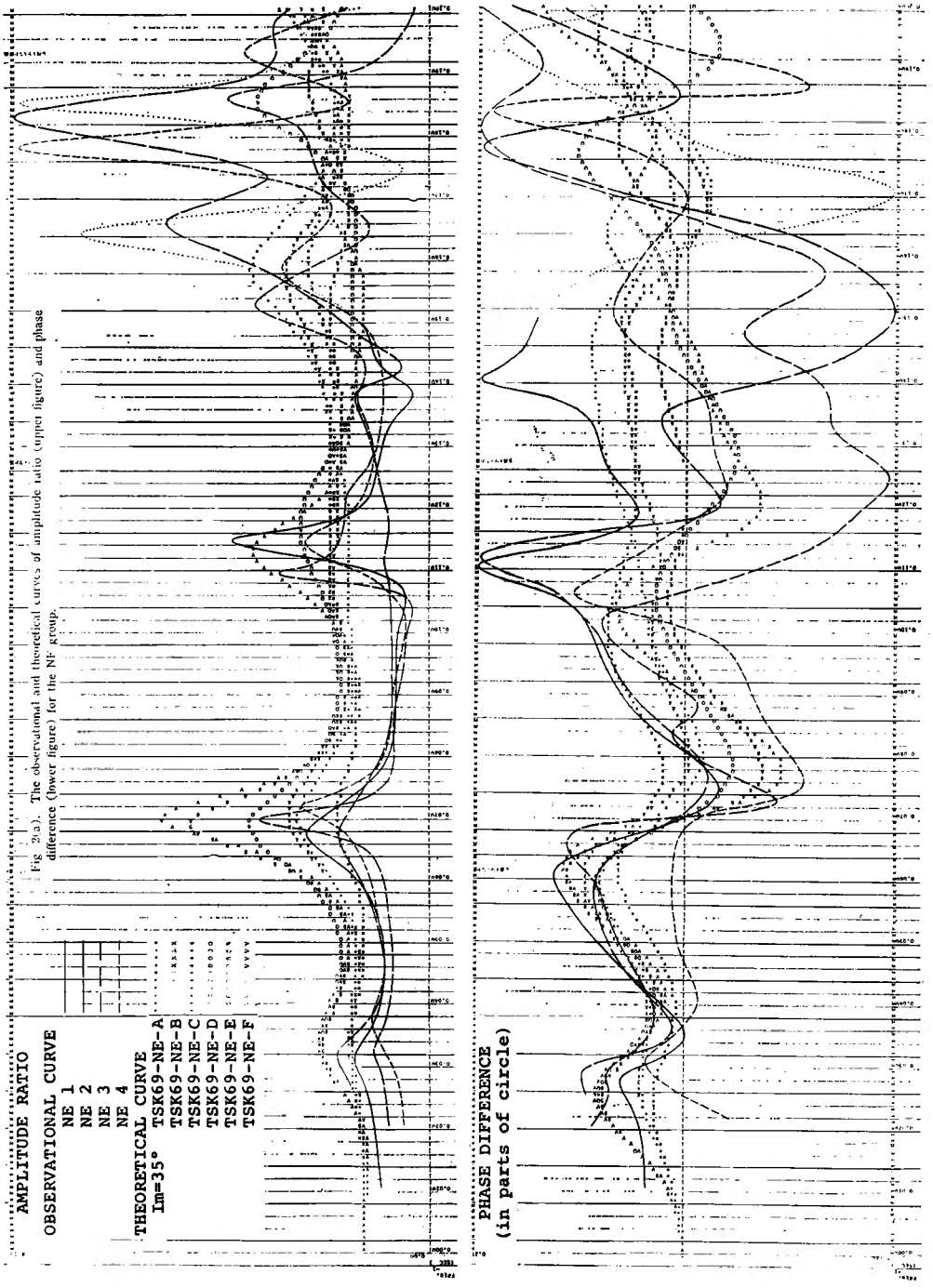

Fig. 2(a). The observational and theoretical curves of amplitude ratio (upper figure) and phase difference (lower figure) for the NE group.

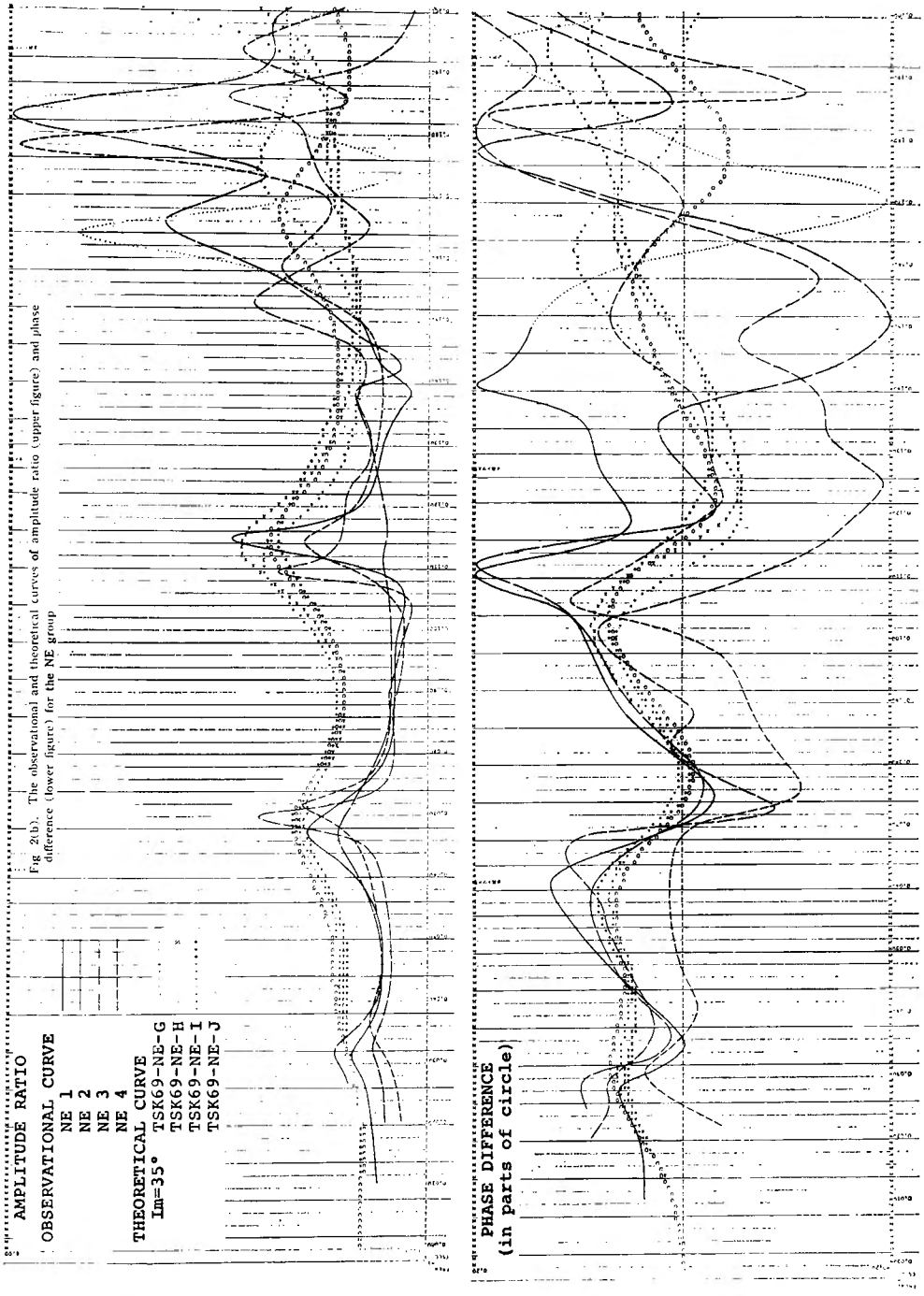

Fig. 2(b). The observational and theoretical curves of amplitude ratio (upper figure) and phase difference (lower figure) for the NE group

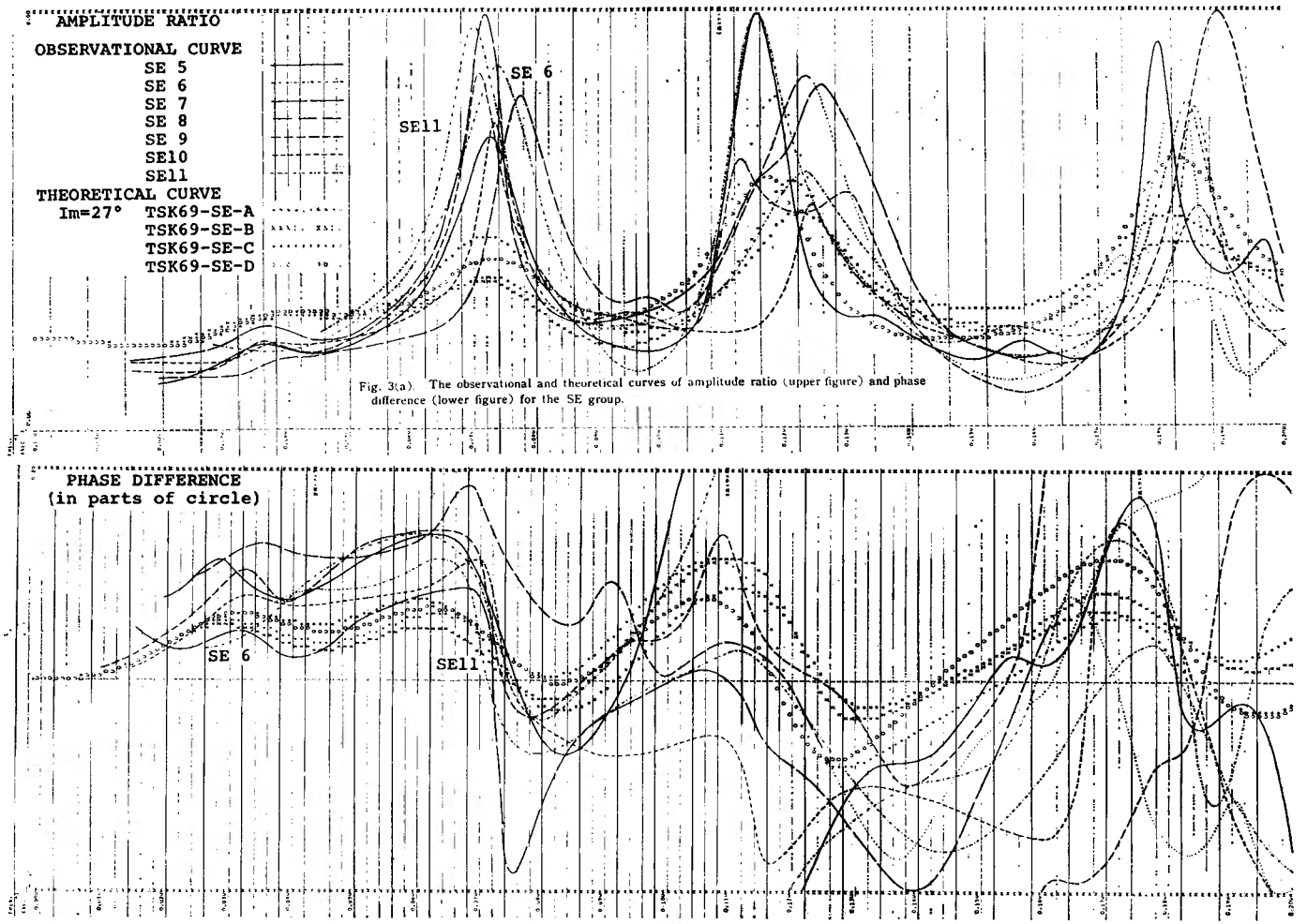

Fig. 3(a). The observational and theoretical curves of amplitude ratio (upper figure) and phase difference (lower figure) for the SE group.

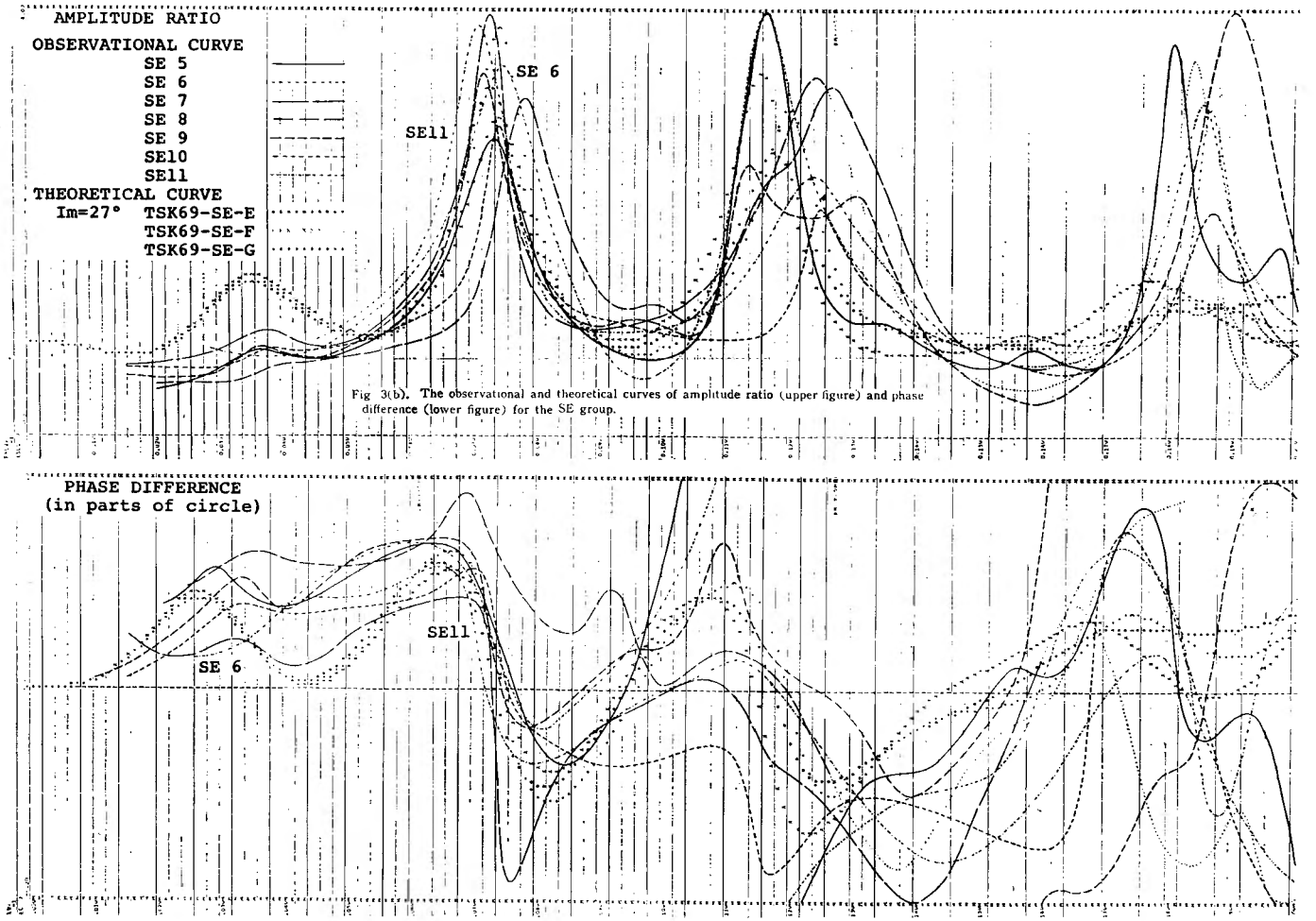

Fig 3(b). The observational and theoretical curves of amplitude ratio (upper figure) and phase difference (lower figure) for the SE group.

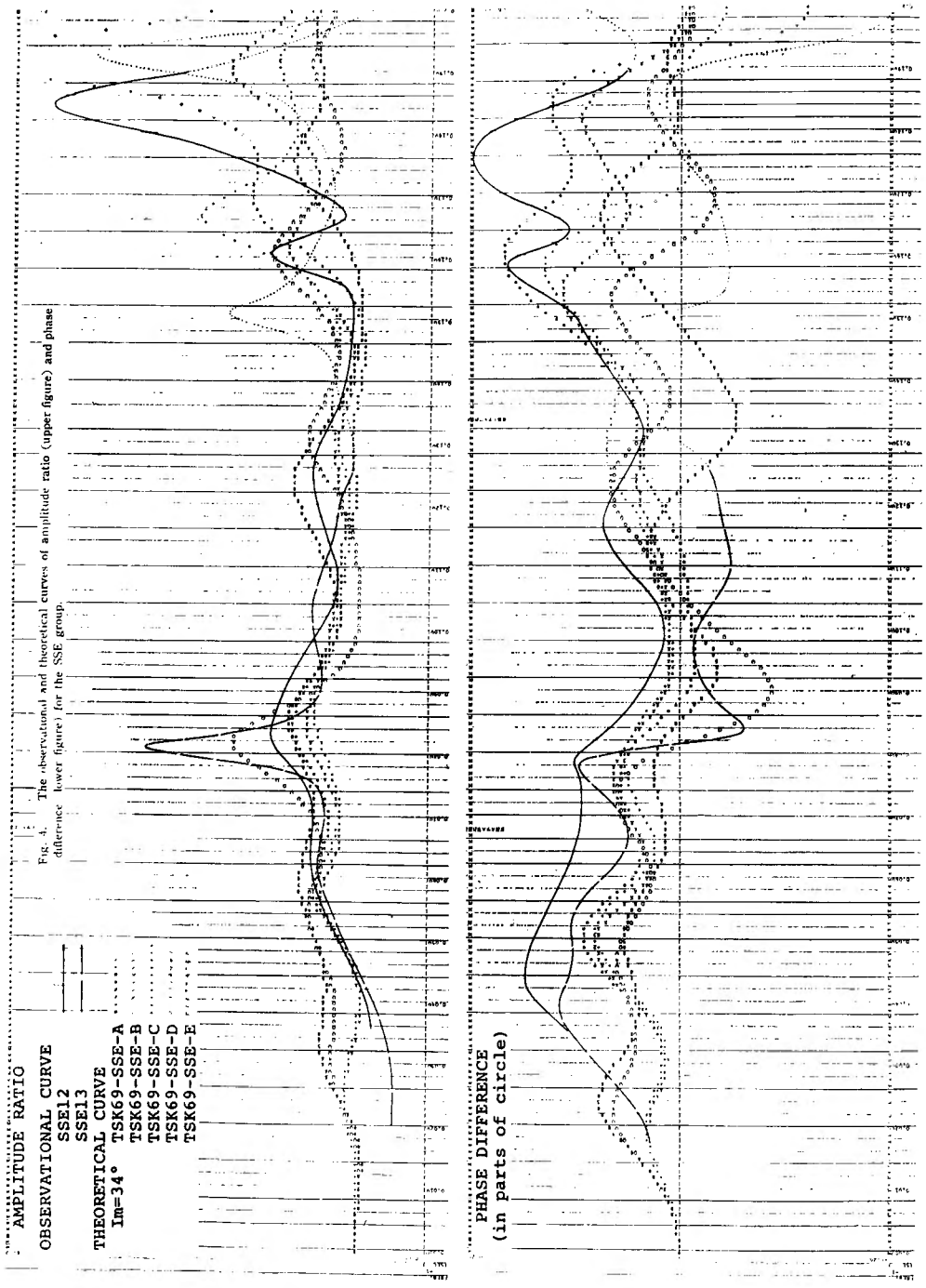

Fig. 4. The observational and theoretical curves of amplitude ratio (upper figure) and phase difference (lower figure) for the SSE group.

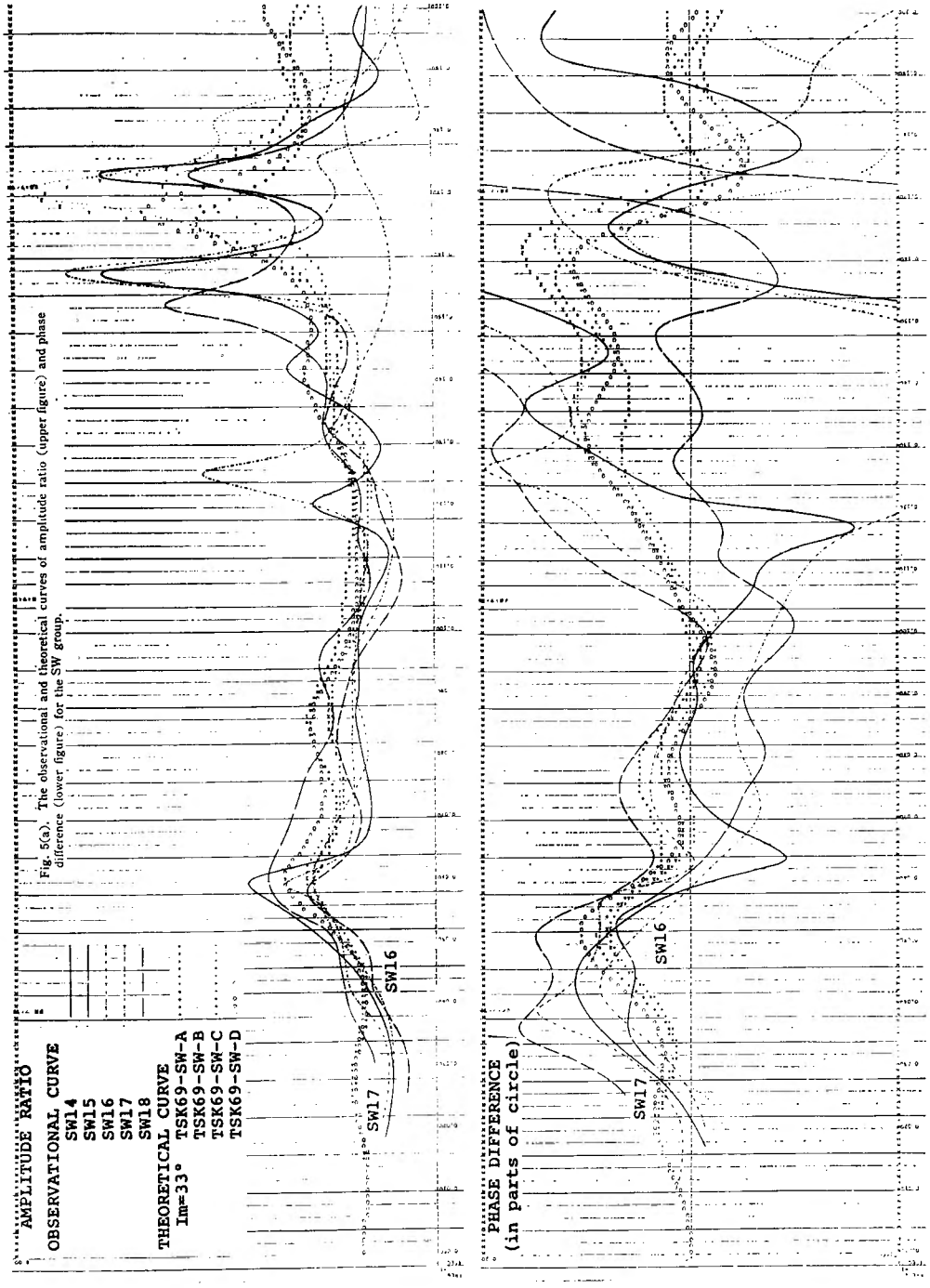

Fig. 5(a). The observational and theoretical curves of amplitude ratio (upper figure) and phase difference (lower figure) for the SW group.

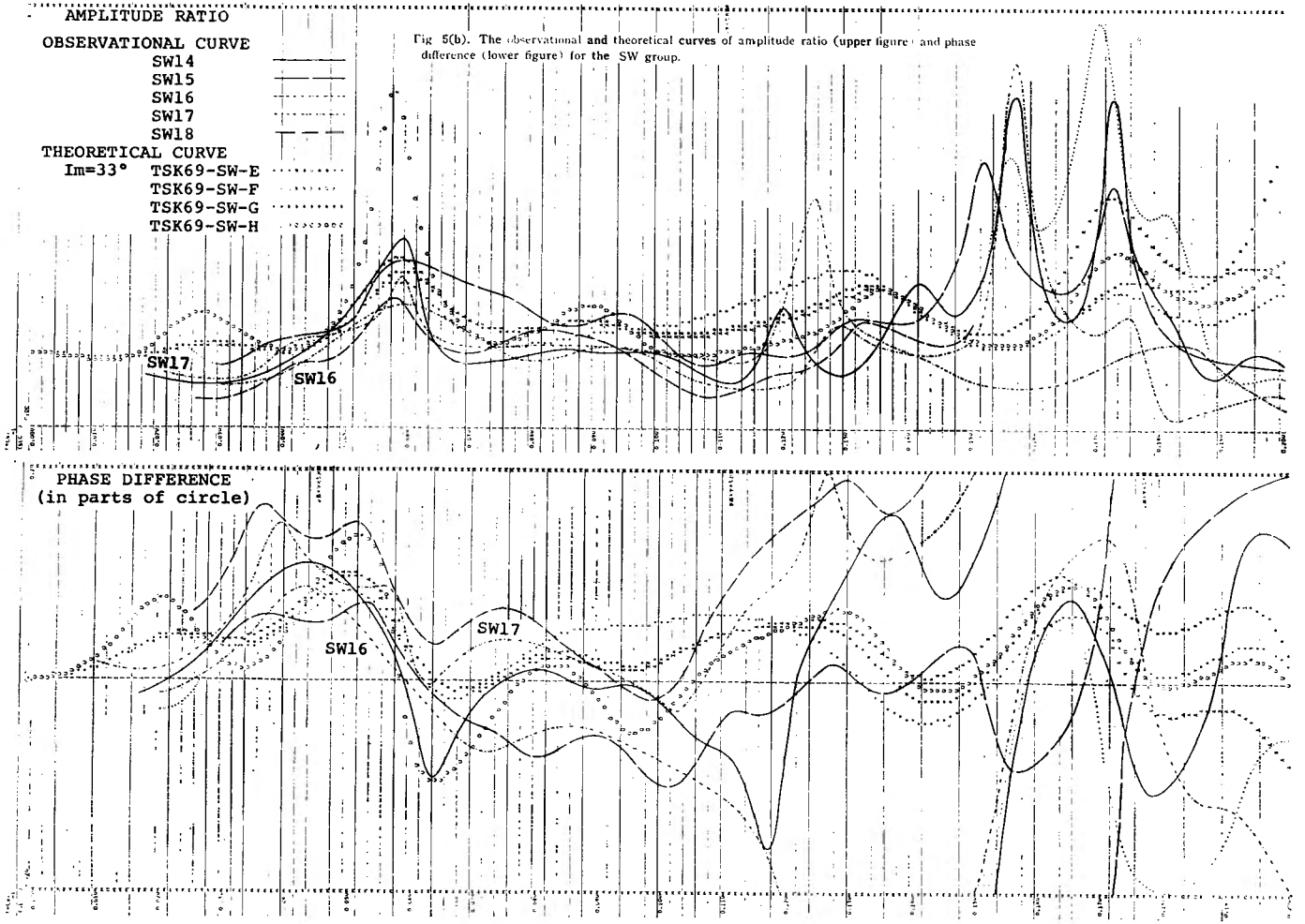

Fig. 5(b). The observational and theoretical curves of amplitude ratio (upper figure) and phase difference (lower figure) for the SW group.

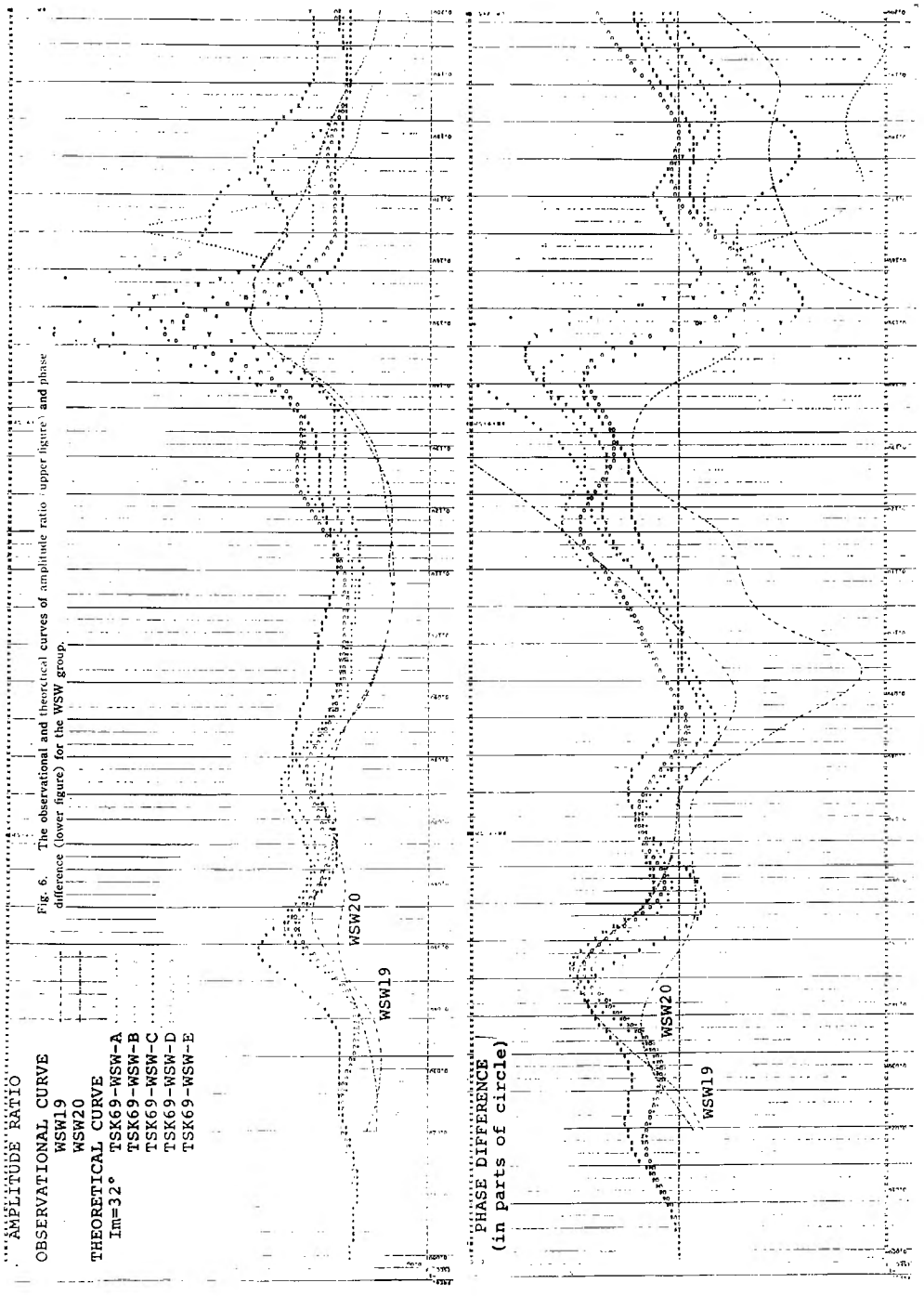

Fig. 6. The observational and theoretical curves of amplitude ratio (upper figure) and phase difference (lower figure) for the WSW group.

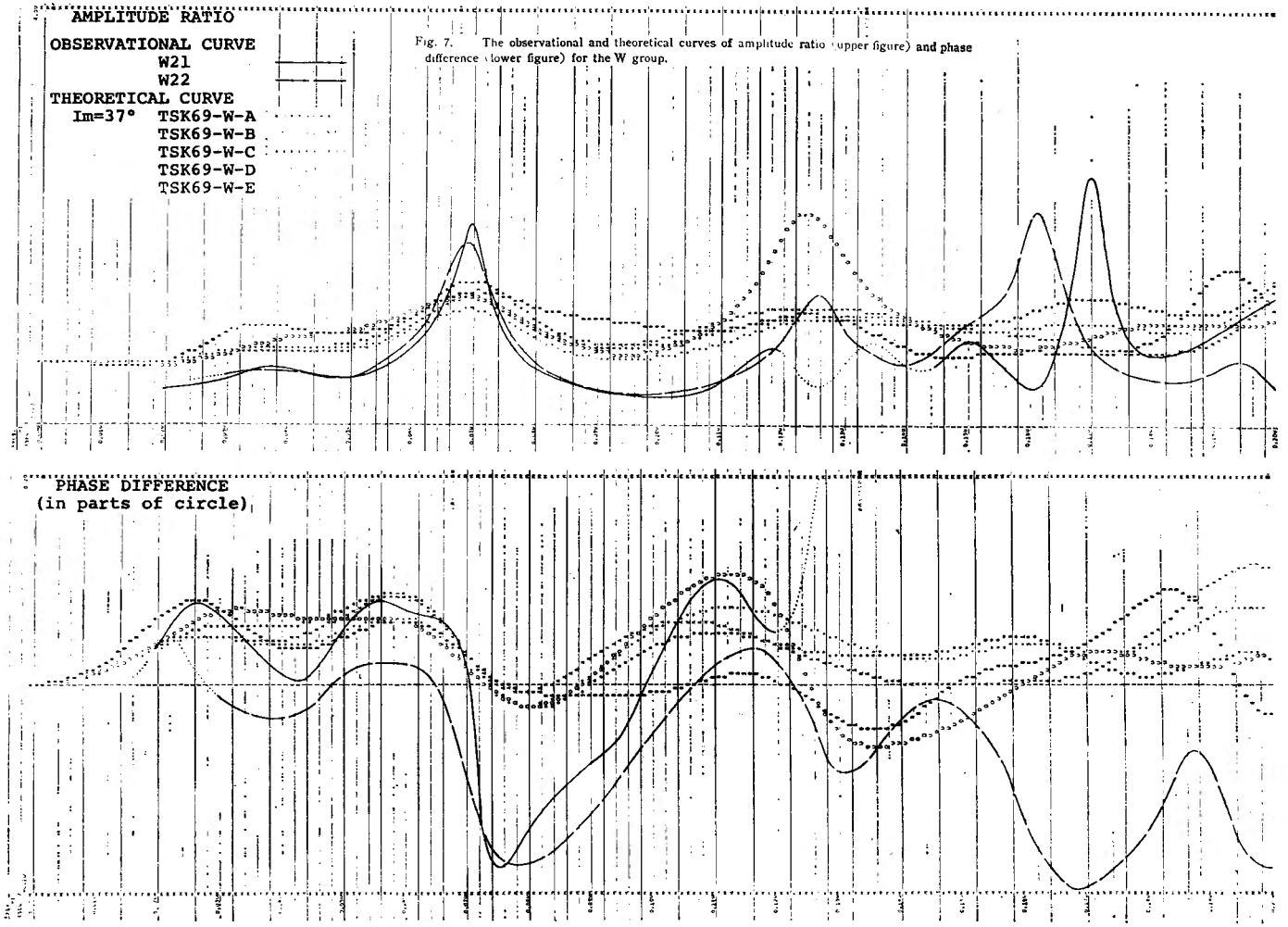

Fig. 7. The observational and theoretical curves of amplitude ratio (upper figure) and phase difference (lower figure) for the W group.

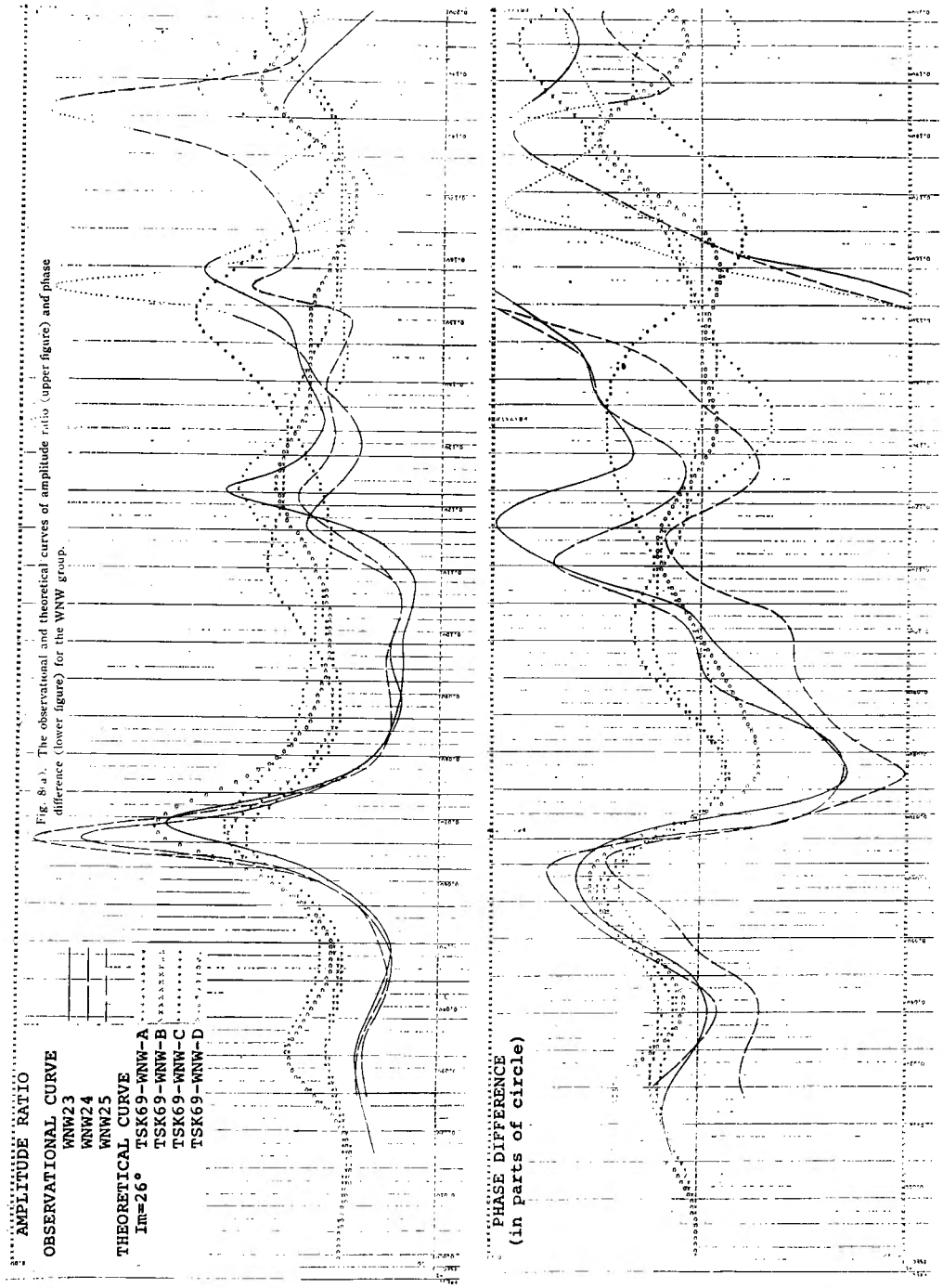

Fig. 8(a). The observational and theoretical curves of amplitude ratio (upper figure) and phase difference (lower figure) for the WNW group.

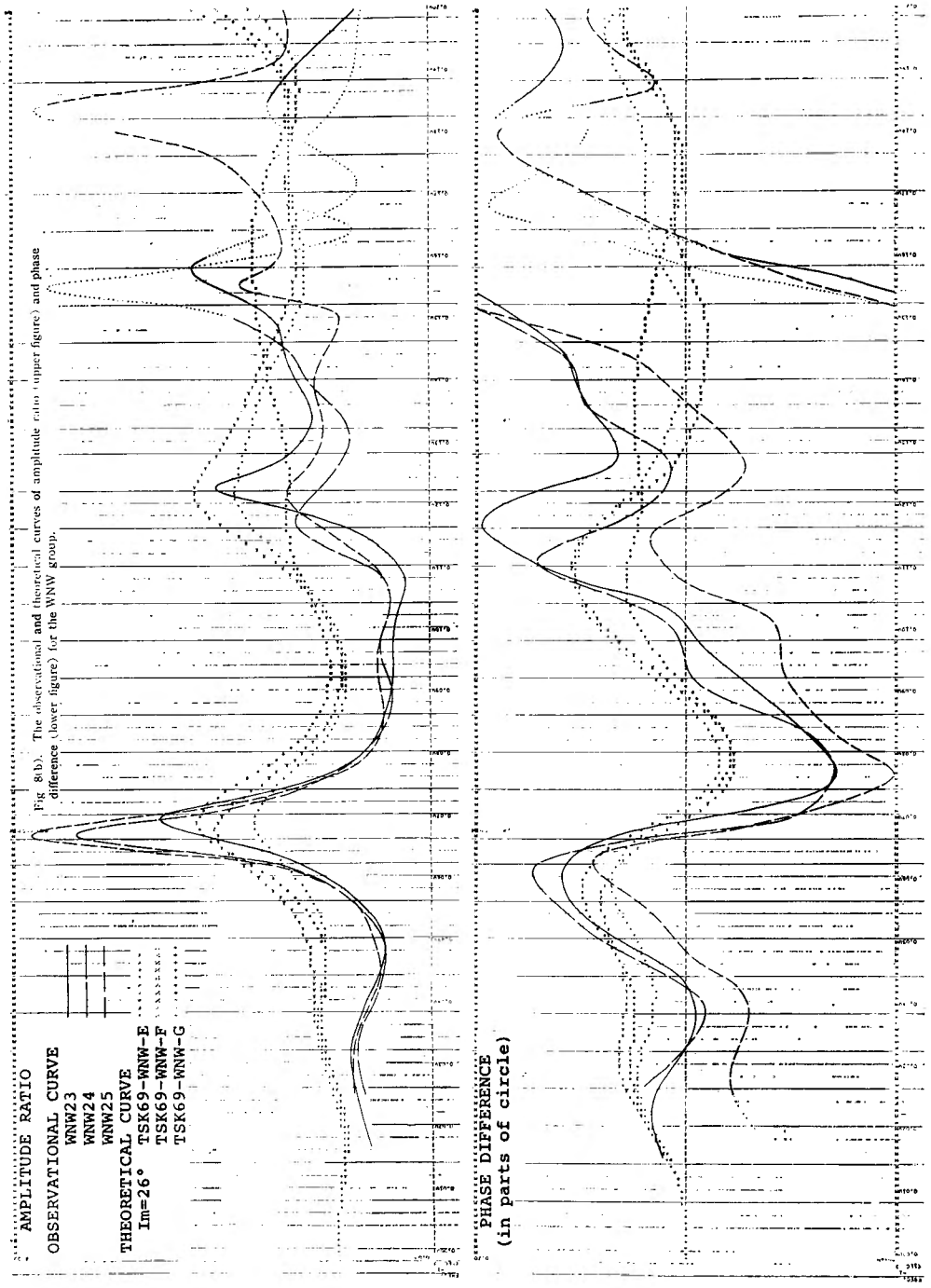

FIG. 8(b). The observational and theoretical curves of amplitude ratio (upper figure) and phase difference (lower figure) for the WNW group.

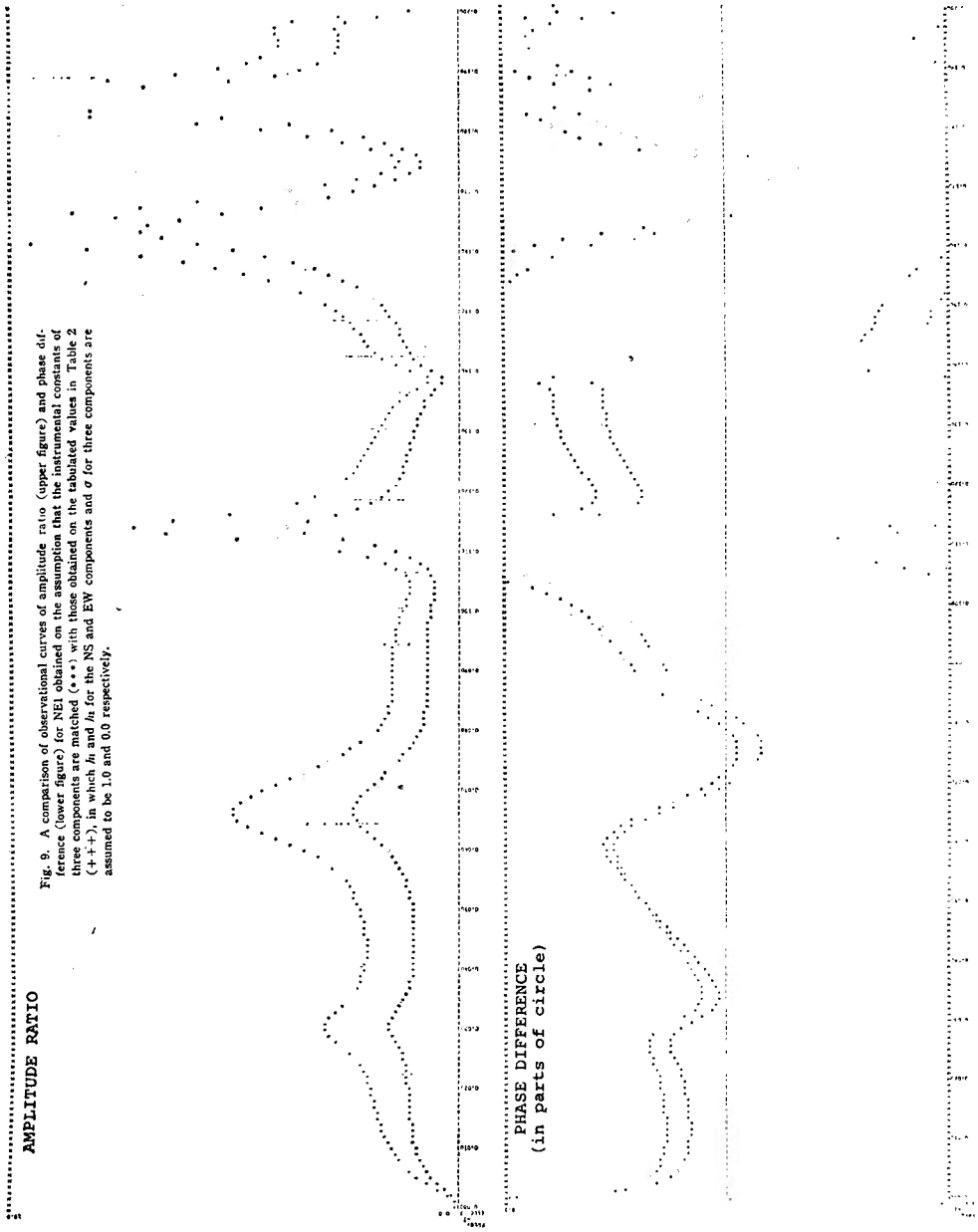

Fig. 9. A comparison of observational curves of amplitude ratio (upper figure) and phase difference (lower figure) for NE1 obtained on the assumption that the instrumental constants of three components are matched (•••) with those obtained on the tabulated values in Table 2 (+++), in which h_1 and h_2 for the NS and EW components and σ for three components are assumed to be 1.0 and 0.0 respectively.

Table 2 gives the instrumental constants of the Columbia long-period seismograph at Tsukuba Seismological Observatory, which are reproduced from its publication. Fig. 9 shows a comparison of observational curves of NE1 obtained on the assumption that the instrumental constants of three components are matched with those obtained on the tabulated values in Table 2, in which h_1, h_2 for the NS and EW components and σ for three components are assumed to be 1.0 and 0.0, respectively. It appears from these figures that no difference in peak positions is noticeable and that discrepancies in the amplitude level between the observational and theoretical curves, particularly of the amplitude ratio, are due to ignoring the difference in the instrumental constants among the components.

Observational curves are generally similar to each other in a group. Although deep-focus shocks are preferable as described in Part 1, there is only one shock, SW18 ($D=600R$ km). It should be noted that the observational curves obtained from SW18 nearly coincide with those obtained from shallow shocks, as is obvious from Figs. 5(a) or (b). This fact substantiates the validity of the above procedure for obtaining observational curves.

An inspection of the observational curves in these figures reveals that they can be divided into two sets based mainly on spacing of peak positions; the NE, SE, W and WNW groups and SSE, SW and WSW groups. In the former groups, the first and second peaks at about 0.35 and 0.70 cps in the amplitude ratio curves and at about 0.25 and 0.60 cps in the phase difference curves are commonly recognized. This fact suggests that the general features of the layering do not very greatly with azimuth in the corresponding azimuthal range. For the SSE, SW and WSW groups, the peak positions are considerably different from the former groups. For the SSE and WSW groups the first peak positions of observational curves are not clear, introducing uncertainties into the results.

3. Determination of crustal and upper mantle structure

Mikumo [1966] studied the crustal structure in Japan by a combined use of gravity anomaly and the surface wave method, based on the travel-time data from explosions. The layer parameters for the eastern Japan, in which Tsukuba is situated in the western part, tabulated in Table 4 in his paper are reproduced in Table 3 (except for the layer thickness). Of the layer parameters of his proposed models, varying only the layer thicknesses, we searched models for each shock group for which the observational curves obtained in section 2 and the theoretical curves calculated from the layer parameters would fit well with each other. For the surface 5.5 km/sec layer, the thickness of 5 km

Table 3. Possible layered structure in the seven regions of the Kanto plain in Japan.

Model	Layer / Parameter	1	2	3	4	M	Crustal Thickness (1+2+3)	Total Thickness (1+2+3+4)	Quality of Obs. Curve	Quality of Fit	Reference
TSK69-	α (km/sec)	5.50	6.05	6.60	7.40	8.00	—	—	—	—	—
	β (km/sec)	3.10	3.40	3.70	4.15	4.50	—	—	—	—	—
	ρ (g/cm^3)	2.50	2.65	2.85	3.10	3.30	—	—	—	—	—
NE-A	H (km)	5	5	2	51	—	12	63	A	B	Fig. 2
+NE-B		5	9	10	36	—	24	60		B	(a)
NE-C		5	4	16	35	—	25	60		B	
NE-D		5	24	19	12	—	48	60		B	
NE-E		5	20	25	9	—	50	59		B	
NE-F		5	23	24	0	—	52	52		B	
NE-G		5	11	13	29	—	29	58		B	Fig. 2
NE-H		5	10	16	26	—	31	57		B	(b)
NE-I		5	14	13	24	—	32	56		B	
*NE-J		5	18	9	23	—	32	55		B	
*SE-A	H (km)	5	15	8	23	—	28	51	A	AA	Fig. 3
SE-B		5	3	22	23	—	30	53		A	(a)
SE-C		5	8	17	22	—	30	52		A	
SE-D		5	13	12	21	—	30	51		A	
SE-E		5	22	20	5	—	47	52		B	Fig. 3
SE-F		5	25	17	3	—	47	50		B	(b)
SE-G		5	21	22	0	—	48	48		B	
SSE-A	H (km)	5	13	0	58	—	18	76	C	C	Fig. 4
+SSE-B		5	9	5	59	—	19	78		C	
SSE-C		5	7	8	55	—	20	75		C	
SSE-D		5	17	23	27	—	45	72		C	
SSE-E		5	25	15	21	—	45	66		C	
+SW-A	H (km)	5	9	7	54	—	21	75	A	C	Fig. 5
SW-B		5	3	14	51	—	22	73		C	(a)
SW-C		5	0	18	49	—	23	72		C	
SW-D		5	13	6	48	—	24	72		C	
SW-E		5	12	11	42	—	28	70		C	Fig. 5
*SW-F		5	15	9	41	—	29	70		C	(b)
SW-G		5	8	17	40	—	30	70		C	
SW-H		5	22	35	5	—	62	67		C	
WSW-A	H (km)	5	17	0	60	—	22	82	C	B	Fig. 6
WSW-B		5	13	6	57	—	24	81		B	
WSW-C		5	6	14	57	—	25	82		B	
+WSW-D		5	9	11	56	—	25	81		B	
WSW-E		5	20	13	41	—	38	79		C	

*W-A	H (km)	5	15	7	29	—	27	56	B	A A	Fig. 7
+W-B		5	9	13	32	—	27	59		B	
W-C		5	3	20	30	—	28	58		A	
W-D		5	20	4	24	—	29	53		B	
W-E		5	24	15	15	—	44	59		B	
WNW-A	H (km)	5	5	15	35	—	25	60	A	B	Fig. 8
+WNW-B		5	11	11	31	—	27	58		B	(a)
WNW-C		5	23	17	14	—	45	59		B	
WNW-D		5	20	22	12	—	47	59		B	
(*)WNW-E		5	15	6	29	—	26	55		B	Fig. 8
*WNW-F		5	18	5	26	—	28	54		B	(b)
WNW-G		5	4	19	28	—	28	56		B	

in Mikumo's model which is based on the explosion seismological study has not been varied, since variation in the thickness of this surface layer does not affect the results over the lower frequency range now considered. The theoretical curves have been computed for average incident angles for the shocks in each group. They are 35°, 27°, 34°, 33°, 32°, 37° and 26° for the NE, SE, SSE, SW, WSW, W and WNW groups respectively.

In the matching process, the fit of the second peak has been considered as most important, since the position of this peak is not much affected by small changes in layer parameters other than the crustal thickness (the sum of layer thicknesses except for the fourth layer) as well as the thickness of the intermediate layer (the fourth layer), and it is reliable compared with the first one (the lowest-frequency peak) with low amplitudes and with low magnification of the instrument for this frequency. Among thousands of test models, seven sets of the models have been selected and tabulated in Table 3, and the corresponding theoretical curves have been plotted on lineprinter papers with observational curves in Figs. 2, 3, 4, 5, 6, 7 and 8. In Table 3, the results of comparison of the observational and theoretical curves are also given in the "Quality of Fit" with the "Quality of Observational Curves". The best, good, fair and poor fits are expressed by rank AA, A, B and C, respectively. The results for each group are examined in the following.

(1) NE group

Spacing of the fourth peak at about 0.16 cps and the fifth peak at about 0.18 cps in the observational curves of amplitude ratio is too close to obtain the corresponding theoretical curves. As is apparent in Fig. 2(a), the third peaks of theoretical curves for models, NE-A, B and C are not so clear as in the case of the observational curves. Theoretical curves of NE-D, E and F

generally agree well with the corresponding observational curves, particularly for lower frequencies. But a thick crustal layer, as much as about 50 km, is not in accord with the results obtained from other studies. For NE-G, H, I and J in Fig. 2(b), the first peaks of the observational curves of amplitude ratio are not in agreement with those of the theoretical curves, in spite of the matching of lower frequency peaks in the phase difference curves. Thus, it follows that there are no models giving a complete matching of the observational and theoretical curves. The most probable model should be selected from models, NE-A, B, C, G, H, I and J, taking into account a consistency with those of other groups.

(2) SE group

For models, SE-A, B, C and D in Fig. 3(a), the peak positions of the observational and theoretical curves coincide fairly well. Among these four models, SE-A is most probable, since the peaks except for the first peak, of theoretical amplitude ratio are of almost the same height as in the observational curves. Theoretical curves of SE-E, F and G in Fig. 3(b) generally coincide well with the observational curves, except that the height of the first peak of theoretical amplitude ratio is too high and that the first peak position of the phase difference does not match well. These three models with a thick crust over 45 km are not substantiated from other studies.

(3) SSE group

There are only two utilized observational curves with a rather low consistency between them. Furthermore, the first peaks in the observational curves are not apparent, and might correspond to the second peaks in the theoretical ones as shown in Fig. 4. Then, high reliability for resultant models is not expected. SSE-D and E with a crustal thickness of 45 km are not substantiated from the other studies. Crustal thicknesses of about 20 km for SSE-A, B and C are rather thin compared with those for the other groups.

(4) SW group

The splitting of peaks at about 0.165 cps on some observational curves of the amplitude ratio and at about 0.045 cps on those of the phase difference as seen in Figs. 5(a) or (b) cannot be substantiated from the corresponding theoretical curves. The first peaks in the observational curves are not in accord with those in the theoretical ones. Thus, a high reliability cannot be expected for the resultant models. Disregarding these facts, the observational curves nearly coincide with the theoretical ones. It is fairly difficult to select the most probable model from SW-A, B, C and D in Fig. 5(a) and SW-E, F and G in Fig. 5(b).

(5) WSW group

There are only two utilized observational curves of rank C. Furthermore, the position of the first peak is obscure, so that the reliability for the resultant models is low. The selection of the most probable model from WSW-A, B, C and D in Fig. 6 is difficult.

(6) *W group*

Although there are only two utilized observational curves of rank B they are comparatively consistent with each other and match with the theoretical curves. Among the four probable models, W-A, B, C and D, the model W-A is most probable from the relative height of the peaks of amplitude ratio, as is apparent in Fig. 7.

(7) *WNW group*

The observational curves are consistent with each other as is apparent in Figs. 8 (a) or (b). Matching between the observational and theoretical curves are not good for models WNW-A and B, in which the position of the third peak does not accord with the corresponding theoretical peak position. Matching is rather good for models WNW-C and D, but these models are not substantiated from other studies. For models WNW-E, F and G, the position of the third peak nearly accords with the observational curves, although the position of the first peak does not completely match. It is difficult to select the most probable model from WNW-A, B, E, F and G.

From the above, the most probable model for each group may be selected on a leading principle that physically the structure does not vary greatly with azimuth. This is partly substantiated from a consistency between the observational curves among the shock groups as seen in the last part of section 2.

As the most probable models for SE and W groups, SE-A and W-A have been selected respectively. In these models the thicknesses of each layer are very similar to one another as is apparent in Table 3. If we extend this characteristic to the other groups without postulating a strict matching of the first peak position, we can propose NE-J, SW-F and WNW-F or possibly E for the corresponding groups. The proposed models are marked with "*" in the first column of Table 3 and shown schematically in Fig. 10. If we pay attention to a strict matching of the first peak position, with disregard of the good matching of higher frequency peaks, we can select W-B, WNW-B and NE-B for the corresponding groups. Extending this characteristic to the other groups, on the assumption that the structure does not vary greatly with azimuth, we can select WSW-D, and, though not with certainty, SW-A and SSE-B for the corresponding groups. The selected models are marked with "+" in the first column of Table 3. In the latter case, the crustal thickness and the thickness

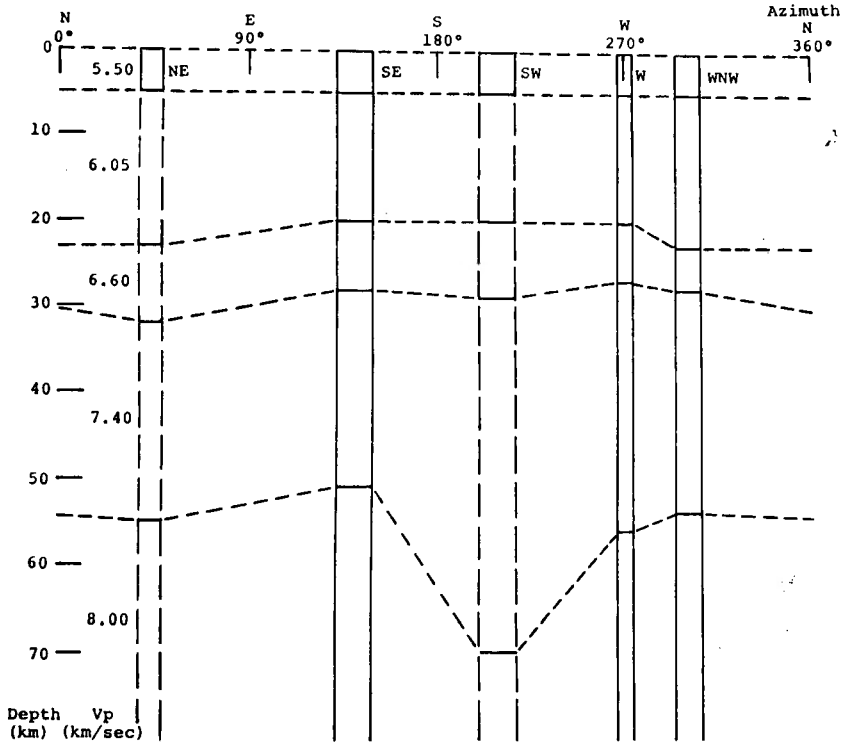

Fig. 10. Most probable layered structure under the Kanto plain.

of the intermediate layer varies from 19 to 27 km and from 31 to 59 km with azimuth respectively, becoming thinner as they approach a direction almost due south. The former case is more probable, in which the crustal thickness and the thickness of the intermediate layer very from 28 (or 26) to 32 km and from 23 to 41 km respectively. The possibitity of other combinations of the models cannot be ruled out. However, for any combinations of the models the average crustal thickness is about 24 to 29 km.

The average crustal thickness of about 29 km in the most probable models is in good agreement with Mikumo's estimation of 27-31 km in the southeast Kanto, and about 30 km estimated by Kaminuma and Aki [1963] from surface wave studies and by Kanamori [1963a] from gravity anomalies. However, a thick intermediate layer over 20 km does not agree with Mikumo's results [1966] that in the eastern part of Japan the intermediate layer might be absent or at most 10 km in thickness. The structure is qualitatively in accord with Aki's proposition [1961] that the intermediate layer of 7.5 km/ses is kept constant from the top of the mantle down to the upper mantle, and Kanamori's indication [1963b] from surface wave studies that the thickness of the inter-

mediate layer is over 20 km almost everywhere in Japan.

4. Discussion and conclusion

We do not repeat in detail the examination of the effects of variation in layer parameters except the thickness, for it was discussed in Part 1. Here we examine another model so far proposed for this area.

Usami *et al.* [1958] and Matuzawa *et al.* [1959] investigated the crustal structure in this area from travel-time curves of explosions. They obtained a layered structure of 5.5 km/sec layer with a 4 to 6 km thickness, 6.1 km/sec layer with a 19 to 23 km thickness and 7.7 km/sec for the uppermost mantle velocity. Theoretical curves on this model were compared with observational curves by varying layer thickness. However, suitable models could not be obtained.

For SE group, adopting 7.7 km/sec instead of 7.4 km/sec for P-wave velocity in the fourth layer and changing appropriately S-wave velocity and density, we searched suitable models. Layer thicknesses and the total thickness of these models were found to be consistent with those in Table 3 with the variation of at most 2 km, though the "Quality of Fit" was rank C.

For SW group, effort was made to attain the matching of the first peak by varying all of the layer parameters in the fourth layer and mantle in the probable range, but this was not successful. Other models with different velocity-density structure or with interleaved soft thin layers postulated by Aki [1968] under the Japan arc may explain the observational curves. This will be examined in Part 3 [Kurita, 1970]. There remains a possibility that the layer interfaces are so inclined that the observational curves may not be explained by any models of horizontal parallel layering. Ishii and Ellis [1969] studied the theoretical curves of amplitude ratio for the dipping layer interfaces, and showed that the curves for dip angles within about 10° are almost the same as those for horizontal parallel layering for such low frequencies as now in consideration. Then the above possibility is very low.

Fig. 11 shows the horizontal stretch of the length of path when a plane wave is incident at the base of strata for five directions of wave approach when the layered structure obtained in section 3 is taken. The shaded and hatched areas correspond to the case when the wave is incident at the upper and lower interfaces of the intermediate layer respectively. When a wave incident at the lower interface of the intermediate layer, reflects one time at the earth's surface, reflects again at the lower interface of the intermediate layer, and then is incident at the station, it travels through the horizontal stretch of the path

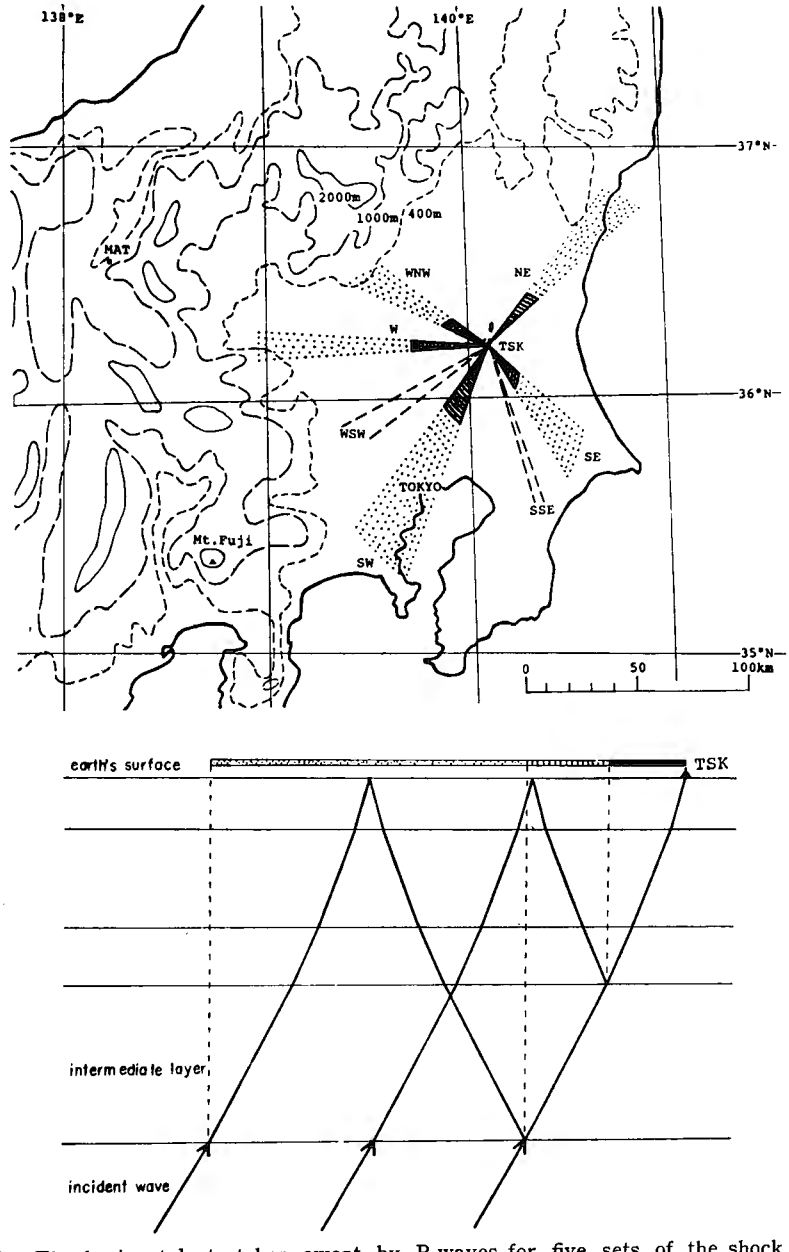

Fig. 11. The horizontal stretches swept by P-waves for five sets of the shock groups when it is assumed that a plane wave incident at the upper (shaded area) and lower (hatched area) interfaces of the intermediate layer is incident at TSK, and when a plane wave, which is incident at the lower interface of the intermediate layer, reflects one time at the earth's surface and then reflects again at the lower interface (dotted area) of the intermediate layer, is incident at TSK, with the contour lines. The corresponding layered model and ray paths are shown in the lower half.

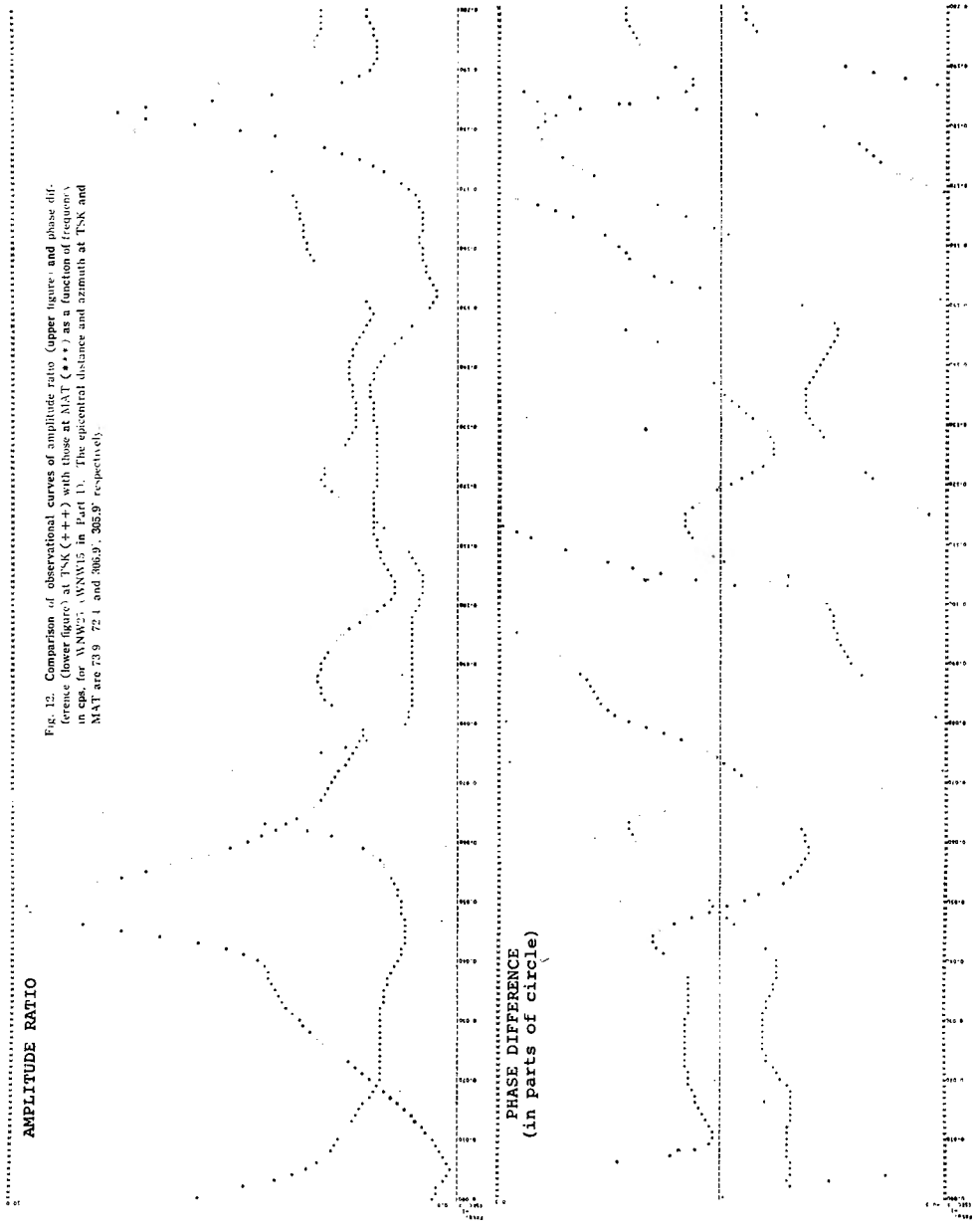

Fig. 12. Comparison of observational curves of amplitude ratio (upper figure) and phase difference (lower figure) at TSK (+++) with those at MAT (•••) as a function of frequency in cps, for WNW15 in Part 1). The epicentral distance and azimuth at TSK and MAT are 739, 72.1 and 306.9°, 305.9° respectively.

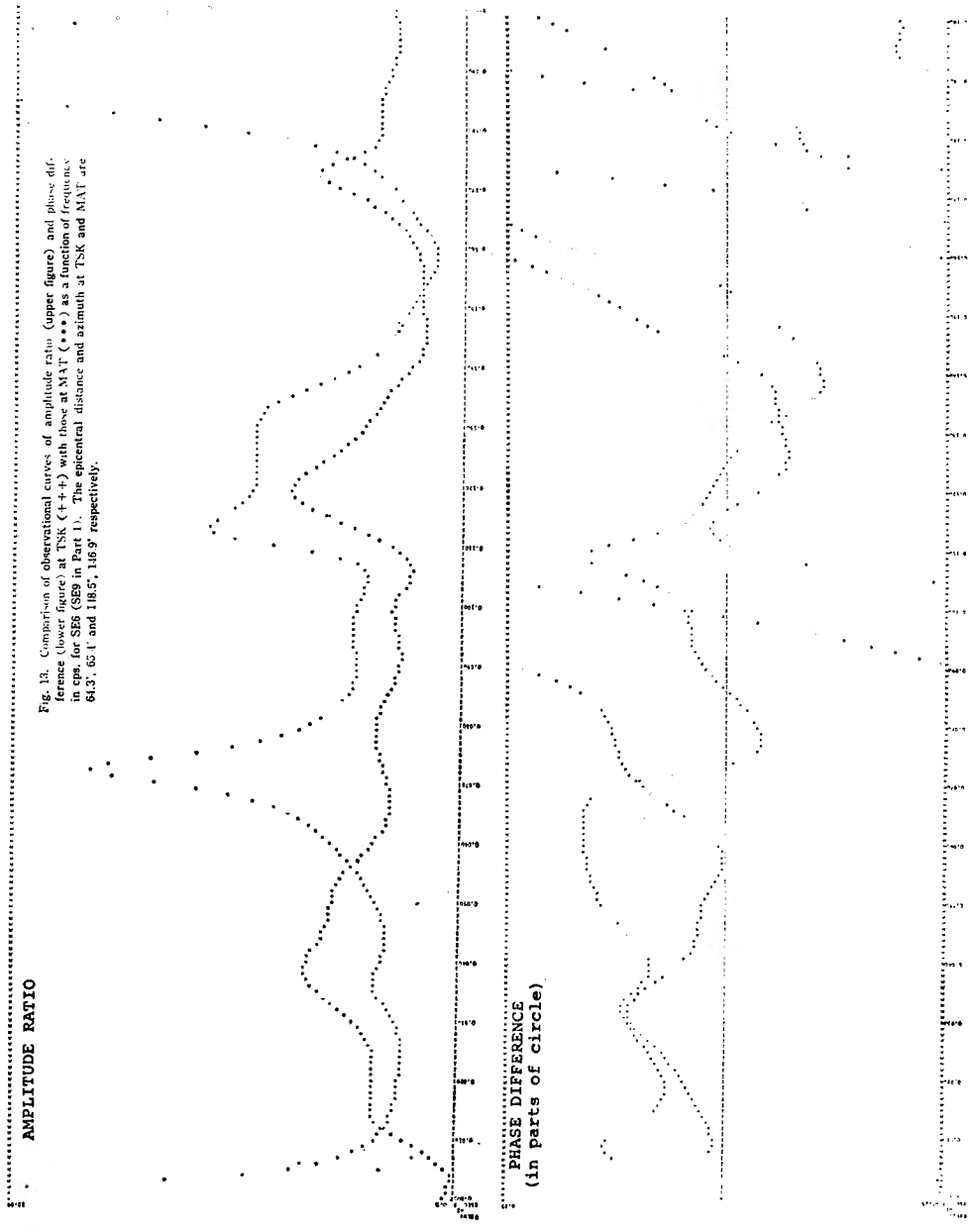

Fig. 13. Comparison of observational curves of amplitude ratio (upper figure) and phase difference (lower figure) at TSK (+++) with those at MAT (***) as a function of frequency in cps. for SE6 (SE9 in Part 1). The epicentral distance and azimuth at TSK and MAT are 64.3°, 65.1° and 118.5°, 146.9° respectively.

with the dotted area. The corresponding layered model and ray paths are shown schematically in the lower half of the figure.

The observational curves of NE, SE, W and WNW groups are similar to each other, suggesting almost the same structure under these regions, which has been substantiated by the similarity of resultant models. These curves, however, differ from those of SSE, SW and WSW groups. This implies a different structure under these two areas, although the models for SSE, SW and WSW groups are not necessarily reliable because of the lack of reliable observational curves or the unmatching of the observational and theoretical curves. Except for SSE and WSW groups whose "Quality of Record" is rank C in Table 3, the resultant models for the SW region show that the thickness of the intermediate layer is different, but the thicknesses of other layers do not differ greatly from those of other models. When the obtained structure in this plain area is compared with that in the central mountain area mentioned in Part 1, the crustal thickness of the former is on an average 10 km thinner than that of the latter and the thickness of the intermediate layer of the former is on an average by several km thinner than that of the latter.

There are four shocks commonly used for the analysis in this paper and in Part 1. Comparisons of the observational curves at TSK with those at MAT are shown in Fig. 12 for WNW25 (WNW15 in Part 1) and in Fig. 13 for SE6 (SE9 in Part 1). The arrival time of later phases is not greatly different between two stations, for the epicentral distance and azimuth are almost the same for MAT and TSK as seen in Table 1 in this paper and Table 2 in Part 1. Then the time interval of analysis is commonly taken as 100 seconds. As is apparent in Fig. 12, the first large peaks appear at about 0.05 and 0.04 cps for the observational curves of amplitude ratio and phase difference at MAT respectively, and at about 0.07 and 0.06 cps for those at TSK, suggesting that the total crustal thickness of TSK is thinner than that of MAT. This is just the same as the case discussed above. In Fig. 13, the difference of two curves is conspicuous over rather lower frequencies, implying a fairly large difference in the structure under two regions.

Fig. 14 shows the Jeffreys-Bullen travel-time residuals for shocks whose epicentral distances are over 30° at MAT and TSK. It is obvious from the figure that at MAT the travel-time residuals do not show any conspicuous azimuthal variations, but at TSK the residuals change sharply from positive to negative between about 130° and 230° in azimuthal range. If we divide these shocks into two groups, namely those from 130° to 175° and those from 175° to 230° in the azimuthal range, the average residuals at MAT and TSK can be tabulated as follows. In the table the values in parentheses show the number

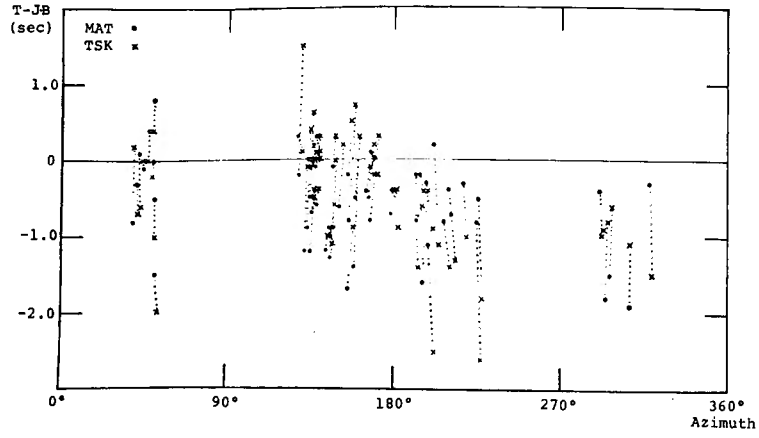

Fig. 14. Comparison of Jeffreys-Bullen travel-time residuals, observed minus computed (T−J·B) at TSK with those at MAT, as a function of azimuth. Rosiduals at these two stations for the same shocks which occurred from April, 1967 to December, 1968 are chained by dottes lines. Data ware obtained from the USCGS earthquake data reports.

of shocks utilized.

Azimuth (deg) / Δ (deg)	130° ~ 175° MAT	TSK	175° ~ 230° MAT	TSK
34° ~ 78°	−0.5 (31)	0.0	−0.5 (15)	−1.1
38° ~ 57°	−0.7 (14)	−0.1	−0.6 (12)	−1.0

As the differences in incident azimuth and epicentral distance between MAT and TSK are within 3° and 1.5° respectively, the incident wave can be considered to have passed through approximately the same portion of the mantle. Therefore, the observational results can not be attributed to the deep mantle structure where the wave passed through, but attributable to the difference in the crustal and upper mantle structure under TSK and MAT. Although at MAT the azimuthal variation of travel-time residuals is not noticed, at TSK waves from south to southwest direction arrive as much as 1.0 seconds earlier than those from south to southeast direction. For the other directions data are insufficient. The above fact may be reduced to a higher velocity in the upper mantle under the southwest part of the Kanto plain, compared with the velocity under the southeast part.

As seen in Part 1, a sharp interface can be replaced by a transitional interface. For a fairly thick intermediate layer, it may be reasonable to consider that the velocity of the uppermost mantle in this area is considerably low (7.4 km/sec) and gradually increases to the velocity in the normal mantle (8.0 km

/sec).

Acknowledgements

This study was begun when the author was a graduate student at the Geophysical Institute, Faculty of Science, Kyoto University. The author is grateful to Dr. Takeshi Mikumo not only for his interest and advice, but also for the stimulating discussions he had with him. The author also acknowledges Prof. Takahiro Hagiwara, the former director of the Earthquake Research Institute, University of Tokyo, for permitting to analyze seismograms recorded at the Tsukuba Seismological Observatory, and Mr. Takayuki Iwata for furnishing him with copies of them. The computation was carried out on a FACOM 230-60 at Kyoto University Data Processing Center.

References

Aki, K., 1961; Crustal structure in Japan from the phase velocity of Rayleigh waves, Part 1. Use of the network of seismological stations operated by the Japan Meteorological Agency, Bull. Earthq. Res. Inst., **39**, 255–283.

Aki, K., 1968; Seismological evidences for the existences of soft thin layers in the upper mantle under Japan, J. Geophys. Res., **73**, 585–594.

Herrin, E. *et al.*, 1968; 1968 seismological tables for P phases, Bull. Seism. Soc. Amer., 58, Special Number, 1193–1241.

Ishii, H. and R. M. Ellis, 1969; Private communication.

Kaminuma, K. and K. Aki, 1963; Crustal structure in Japan from the phase velocity of Rayleigh waves, Part 2. Rayleigh waves from the Aleutian shock of March 9, 1957, Bull. Earthq. Res. Inst., 41, 217–241.

Kanamori, H., 1963a; Study on the crust-mantle structure in Japan, Part 2. Interpretation of the results obtained by seismic refraction studies in connection with the study of gravity and laboratory experiments, Bull. Earthq. Res. Inst., 41, 761–779.

Kanamori, H., 1963b; Study on the crust-mantle structure in Japan, Part 3. Analysis of surface wave data, Bull. Earthq. Res. Inst., 41, 811–818.

Kurita, T., 1969a; Crustal and upper mantle structure in Japan from amplitude and phase spectra of long-period P-waves, Part 1. Central mountain area, J. Phys. Earth, 17, 13–41.

Kurita, T., 1969b; Spectral analysis of seismic waves, Part 1. Data windows for the analysis of transient waves, Special contributions, Geophys. Inst., Kyoto Univ., No. **9**, 97–122.

Kurita, T., 1970; Crustal and upper mantle structure in Japan from amplitude and phase spectra of long-period P-waves, Part 3. Chugoku Region, J. Phys. Earth, 18. (in press)

Matuzawa, T., T. Matumoto and S. Asano, 1959; On the crustal structure derived from observations of the second Hokoda explosion, Bull. Earthq. Res. Inst., 37, 509–524.

Mikumo, T., 1966; A study on crustal structure in Japan by the use of seismic and gravity data, Bull. Earthq. Res. Inst., 44, 965–1007.

Ritsema, A. R., 1958; $(i-\Delta)$-curves for bodily seismic waves of any focal depth, Meteorol. and Geophys. Inst. Djakarta, Verhandelingen, 54, 1–10.

Usami, T., T. Mikumo, E. Shima, I. Tamaki, S. Asano, T. Asada and T. Matuzawa, 1958; Crustal structure in northern Kwanto District by explosion seismic observations, Part 2. Models of crustal structure, Bull. Earthq. Res. Inst., 36, 102–113.